Switching field distribution of ultradense arrays of single-crystalline magnetic nanowires

A. Pierrot, D. Yi, L. Peres, K. Soulantica, R. Cours, B. Warot-Fonrose, C. Marcelot, M. Respaud, F. Béron, T. Blon

Switching field distribution of ultradense arrays of single crystalline magnetic nanowires

A. Pierrot[1], D. Yi[1], L. Peres[1], K. Soulantica[1], R. Cours[2], B. Warot-Fonrose[2], C. Marcelot[2], M. Respaud[1,‡], F. Béron[3], T. Blon[1,*]

[1] Université de Toulouse, Laboratoire de Physique et Chimie des Nano-Objets, UMR 5215 INSA, CNRS, UPS, 135 Avenue de Rangueil, F-31077 Toulouse, cedex 4, France

[2] CEMES, Université de Toulouse, CNRS, 29 Rue Jeanne Marvig, BP 94347, F-31055 Toulouse, France

[3] Univ. Estadual Campinas, UNICAMP, Inst. Phys. Gleb Wataghin, Rua Sergio Buarque de Holanda 777, BR-13083859 Campinas, SP, Brazil

[‡] Present address : CEMES, Université de Toulouse, CNRS, 29 Rue Jeanne Marvig, BP 94347, F-31055 Toulouse, France

[*] corresponding author : thomas.blon@insa-toulouse.fr

Abstract

Ultra-dense arrays of magnetic nanoelements present considerable interest for extending areal densities in magnetic recording media, provided that they display high switching fields and corresponding low standard deviations. Here, we report the switching field distribution of bottom-up synthesized single-crystalline vertical Co nanowires self-organized in 2D hexagonal superlattices. The combined shape and Co hexagonal compact magnetocrystalline anisotropies in individual nanowires of diameter as small as 6 nm define a robust perpendicular magnetic anisotropy despite important interactions in their superlattices of 10×10^{12} NWs/in². Using quantitative analysis of temperature-dependent first-order reversal curves, we capture the switching field distribution in this dipolar-coupled perpendicularly magnetized nanomagnets. First, the interwire dipolar interactions are treated separately and show a dominant mean field character with temperature independent amplitudes that scale with the nanowire packing fraction. Then, the intrinsic switching field distribution, namely independent of interwire interactions, is determined as a function of temperature in the 5K-300K range. The mean value and deviation are both found to be driven by the intrawire dipolar interaction and the temperature-dependent uniaxial magnetocrystalline anisotropy, but of smaller amplitudes than those expected from bulk behavior. With coercive fields ranging between 0.3 and 0.8 T, the switching field deviations relative to coercivity reach 20% which is a moderate value regarding pitch arrays as small as 8 nm.

Arrays of magnetic nanostructures are key elements of past, present and future of magnetic recording technology [1]. The increasing demand in data storage led to the concept of bit patterned media (BPM) where information should be stored in a single magnetic element in opposite to conventional continuous magnetic media [2]. For large-scale fabrication of BPM, pure bottom-up fabrication methods are considered as exciting alternatives to top-down approaches [3]. Among reported spontaneously organized magnetic nanostructures on substrates, magnetic nanowires (NWs) are particularly suitable due to their intrinsic unidirectional growth [4,5,6]. However, it is still a challenge to stabilize wafer-scale arrays of NW made of magnetically hard structure and regularly packed with densities of more than 10^{12} elements per inch square. Whereas most studies on magnetic NW assemblies concern template-synthesized NWs with low or moderate densities and/or inadequate crystallographic structures [7,8,9], we recently reported the growth and self-organization of magnetic nanowire arrays that fulfill BPM structural constraints. Regular 2D hexagonal lattices of vertical free-standing Co nanowires are immediately produced on a surface using a liquid phase chemical synthesis [10,11]. With tunable diameters in the range 6-12 nm and interwire distances of 2-3 nm, NWs densities of 3 to 10×10^{12} NWs/in^2 are obtained [12]. Since the *c* axis of the hexagonal compact (*hcp*) Co single-

crystal lies along the wire axis, the combination of shape anisotropy and Co *hcp* uniaxial magnetocrystalline anisotropy overcomes important dipolar interactions resulting in a magnetic anisotropy along the NWs, *i.e.* perpendicular to the 2D assembly [12,13]. This system is very promising as it combines bottom-up synthesis of single crystalline nano-elements, self-organization in 2D dense superlattices and robust out-of-plane anisotropy. However, the coercive fields (H_C), around 0.3 T at room temperature, should be enhanced for operational applications. This necessitates the identification of anisotropy dispersion and limitations in the system, ideally independently of dipolar interactions, that is, the determination of the intrinsic switching field distribution (iSFD). Indeed, the SFD deviation $\sigma_{H_{sw}}$ and its relative value $\sigma_{H_{sw}}/H_C$ constitutes fundamental figures of merit of recording media [2]. The measure of the iSFD in interacting nanomagnets remains a complex problem and different approaches have been developed over years such as the $\Delta H(M, \Delta M)$ method [14,15,16] and isothermal remanent magnetization and DC demagnetization remanence analysis [17]. The First-Order Reversal Curves (FORC) technique has been recently proposed for this purpose, in addition to its ability to map and quantify magnetizing and demagnetizing interactions in assemblies [18,19]. Recent studies demonstrated that the determination of the iSFD deviation from a FORC analysis is quantitatively relevant for dipole-coupled nanomagnets [20,21,22]. In the aim of capturing the anisotropy amplitude and its limitations in ultradense arrays of single-crystalline NWs, here we used temperature-dependent FORC analysis in the range 5K-300K. Focusing on two Co NW arrays differing by their NW diameters and packing fractions, we first analyze major hysteresis loops to focus on the coercivity and activation volumes of the magnetization reversal, and we present temperature-dependent FORC analysis to obtain the iSFD, as well as its variation as a function of temperature that allows discussing the anisotropy in the *hcp* Co NWs.

The arrays studied consist of metallic Co NWs naturally covered with organic surfactants. They are synthesized by adapting the seed-mediated solution phase synthesis of nanocrystals [23] to grow them on crystalline thin films, here on epitaxial Pt(111)/Al_2O_3(0001) [24]. Details about the synthesis can be found elsewhere [12]. The whole process leads to the epitaxial growth of vertical single-crystalline wires with the *c*-axis of the Co *hcp* structure parallel to the NW axis [12]. The structural parameters can be tuned by varying the nature of reactants [11] and/or their relative concentration [12]. Here we present two families of NW arrays illustrated by two samples which differ by the solvent used for the synthesis: anisole for hereafter named sample *A*, and toluene for sample *T*. For sample *A*, the length is L = 320 nm and diameter D = 12.5 nm (aspect ratio, AR: 26), whereas L = 180 nm and D = 6.3 nm (AR: 29) for sample *T*. Transmission electron microscopy shown in Fig. 1(a) reveals that NWs of sample *A* possess sharp extremities defining a needle-like shape, whereas NWs of sample *T* (Fig. 2(a)) are more cylindrical but subject to bending due to a smaller diameter. Considering an organic shell of 2.1 nm separating neighbouring wires [11,12], the L/p ratio, with p the NW array pitch, is equal to 22 for both samples, while packing fractions $P = (\pi/2\sqrt{3}).(D/p)^2$ are P_A = 0.66 and P_T = 0.51.
Due to their shape and uniaxial crystalline anisotropies [10,12], the NW arrays present an easy-axis perpendicular to the substrate, *i.e.* parallel to the NWs. This is illustrated by easy-axis major hysteresis loops (MHL) measured perpendicularly to the substrate in Fig. 1(c) (sample *A*) and Fig. 2(c) (sample *T*), whereas loops measured parallel to the substrate correspond to the hard-axis behaviour (Fig. 1(d)-Fig. 2(d)). For both samples, the easy-axis loops are clearly sheared whatever the temperature as a result of the demagnetizing dipolar interaction in the arrays. Note that low temperature $M(H)$ measurements performed after field cooling do not display any exchange bias field suggesting the absence of Co/CoO ferromagnetic/antiferromagnetic coupling, and therefore no or little Co oxidation. The measured absolute values of M_s are constant as a function of temperature (max. 7% variation in the range 5-300 K), as expected for bulk Co.

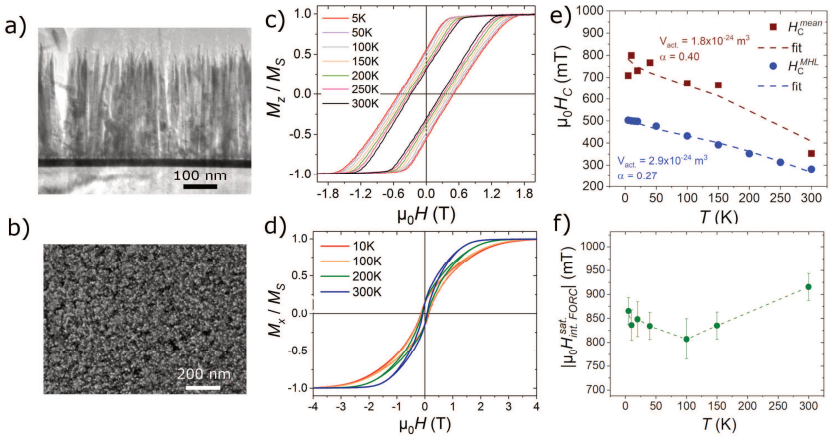

Figure 1 – sample A : a) cross-sectional transmission electron microscope (TEM) and b) scanning electron microscope (SEM) pictures. Magnetic hysteresis loops measured at different temperatures for applied magnetic fields c) parallel (after field cooling), and d) perpendicular to the NWs. e) Coercive fields measured on major hysteresis loops H_C^{MHL} and mean field of the SFD measured on FORC diagrams H_C^{mean} as a function of temperature, and associated fits (Eq. 1). f) $\left|H_{int,FORC}^{sat.}\right|$ extracted from point A of FORC diagrams as a function of temperature (see Fig. 3).

The evolution of the MHL coercive field H_C^{MHL} as a function of temperature is displayed in Fig. 1(e) and Fig. 2(e) for samples *A* and *T*, respectively. Whereas both samples present similar coercive fields of 0.3 T at room temperature, sample *T* and *A* reach 0.8 T and 0.5 T at 5K, respectively. The temperature dependence of H_C^{MHL} is analysed in terms of thermal relaxation within the Sharrock formula [25]: $\mu_0 H_c(T) = \frac{2\alpha K_{eff}(T)}{M_S}\left[1-\left(25k_BT/\alpha K_{eff}(T)V_{act.}\right)^{\frac{1}{2}}\right]$, Eq. 1. The effective uniaxial anisotropy $K_{eff} = K_1(T) + \frac{1}{4}\mu_0 M_s^2$, with $K_1(T)$ is considered to behave as the magnetocrystalline anisotropy constant of *hcp* Co bulk [26], while the second term factor related to the cylindrical shape anisotropy is considered temperature-independent, as M_s. The use of bulk values for K_{eff} did not allow fitting the experimental data. Therefore we introduced a phenomenological parameter α (≤ 1) to define a reduced uniaxial anisotropy αK_{eff} that accounts for the temperature dependence of $H_C(T)$.

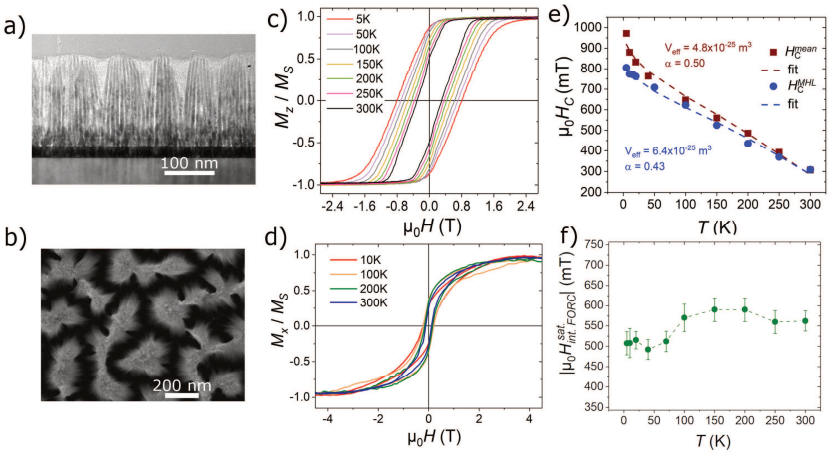

Figure 2 - Sample T : a) cross-sectional TEM and b) SEM pictures of sample *T*. Magnetic hysteresis loops measured at different temperatures for applied magnetic fields c) parallel (after field cooling), and d) perpendicular to the NWs . e) Coercive field measured as a function of temperature and associated fits (Eq. 1). f) $\left|H^{sat.}_{int,FORC}\right|$ extracted from point A of FORC diagrams as a function of temperature (see Fig. 4).

The fits, displayed in Fig. 1(e) and 2(e), were carried out using Eq. 1 with activation volume $V_{act.}$ and α as fitting parameters. The deduced activation volumes are inferior to the nanowire volume ($V_{act.} \approx V_{NW}/14$ (portion of 25 nm in length), $V_{NW}/16$, (21 nm) for samples A and *T* respectively) which indicates that the reversal is localized, as commonly observed in the literature of magnetic nanowires [27,28,29,30,31]. The low values of α demonstrates that the magnetic anisotropy involved in the energy barrier of the magnetization reversal is lower than the theoretical one, but keeps the expected temperature dependence of the Co *hcp* magnetocrystalline contribution.

The FORC diagrams measured on sample *A* and sample *T* in the temperature range 5-300K are displayed in Fig. 3 and Fig. 4, respectively. FORC were measured starting from the positive saturation to reach the field H_r where each FORC was measured scanning back the field H from H_r to the positive saturation field. The FORC diagrams were computed using the equation $\rho_{FORC}(H, H_r) = -\frac{1}{2}\frac{\partial^2 M(H,H_r)}{\partial H_r \partial H}$, Eq. 2, [19] and were normalized with respect to the maximum value ρ^{max}_{FORC} of the considered diagram. For sample *A,* the FORC plots exhibit an identical signature for each temperature: they are mainly composed of an intense interaction field distribution (IFD) almost parallel to the interaction field axis H_{int}. Note that a coercive field distribution (CFD) is also present along the H_c axis at $H_{int} = 0$ (see point C in Fig. 3(b)): this distribution does not represent real switchings but originates from artificial enhancement of intrinsic coercivities due to dipolar interactions [18,19,20,22,32]. The IFD fingerprint is commonly encountered in the literature of nanowire arrays [33][34][35][36][37][38][39][40][41][42][43] and is numerically reproduced in simulations of hysteron assemblies interacting in a demagnetizing interaction field [18,22]. For sample T, the FORC diagrams also consist primarily of an IFD, but gradually change as temperature decreases, to the so-called "wishbone" shape [44], which is most apparent at 5K. It should be noted that sample A exhibits a comparable, albeit milder, gradual bending from the IFD to the wishbone signature at low temperatures. The wishbone shape is a distinguishing feature of systems with demagnetizing mean interaction field and coercive field distribution [22,44]. Therefore, the gradual shift from IFD to low-

temperature wishbone shows that the coercivity distribution has gradually broadened, as explained quantitatively in the following.

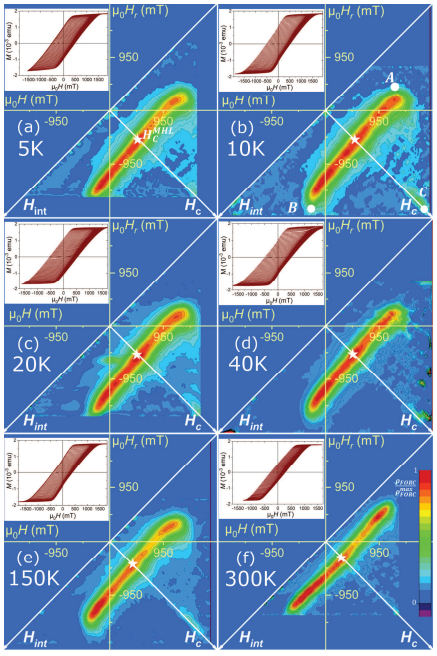

Figure 3: FORC diagrams obtained from measurements (insets) between 5K and 300K on sample *A*. The coercive fields H_c^{MHL} measured on the corresponding major hysteresis loops are reported as star symbols.

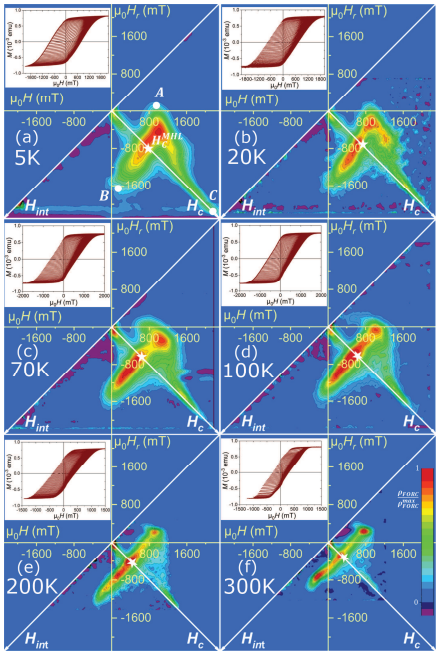

Figure 4: FORC diagrams obtained from measurements (insets) between 5K and 300K on sample *T*.

Quantitative information was obtained from FORC diagrams exploiting the A, B and C point coordinates in the (H_c, H_{int}) plane (Fig. 3(b)). Indeed it has been shown using hysteron simulations that the A, B, C points in the (H_c, H_{int}) plane have coordinates [18,20,22] : A: $(H_c^{min}; \left|H_{int,FORC}^{sat}\right|)$, B: $(H_c^{mean}; H_c^{mean}+H_c^{min} - \left|H_{int,FORC}^{sat}\right|)$, C: $(H_c^{max} + \left|H_{int,FORC}^{sat}\right|; 0)$, where H_c^{min}, H_c^{max} and H_c^{mean} are extremal and mean values of the switching field distribution in the assembly, respectively. Extracted H_c^{mean} values are plotted in comparison with H_c^{MHL} on Fig. 1(e) (sample *A*) and Fig. 2(e) (sample *T*). Whereas H_c^{MHL} values reported on FORC diagrams (see star symbols on FORC diagrams in Fig. 3-4) are very close to the crossing point between IFD and the H_c axis, H_c^{mean} is always larger than H_c^{MHL} on the whole temperature range (Fig. 1(e)-2(e)). H_c^{MHL} refers to the field value for which $M = 0$, whereas H_c^{mean} is the mean value of the switching field distribution. For a symmetrical distribution, both should be equal in the absence of dipolar interaction or in the presence of a mean interaction field. Any difference suggests here that interactions alter coercivity. Both experimental and theoretical works have established that dipolar interaction reduces coercivity because of the stray field of nearby NWs producing an antiparallel local interaction field [23,45,46]. Consequently, the total field is larger than the applied field and $M_z = 0$ is reached before $H_{app} = H_c^{mean}$. For the sample *T*, the contrast between H_c^{mean} and H_c^{MHL} is lower, which is consistent with $P_T < P_A$ and consequently with moderate

interactions in sample *T*. The interaction fields at saturation magnetization $\left|H_{int,FORC}^{sat}\right|$ have been extracted from the coordinate of point A in FORC diagrams and displayed in Fig. 1(f)-2(f). In the moving Preisach model [47], the mean interaction field writes $H_{int}^{zz} = \alpha_m M_z$ with the moving constant $\alpha_m < 0$ for demagnetizing interactions. Recent approaches calculated N_{int}^{zz}, the *z* component of the effective demagnetizing tensor associated to the dipolar interaction field defined as $H_{int}^{zz} = -N_{int}^{zz} M_z$, and demonstrated that $N_{int}^{zz} = P$ for $L/p > 10$ [48,49]. Such a regime prevails in these NWs arrays as supported by ferromagnetic resonance analysis [13]. Consequently, the maximum interaction field is expected at saturation with $H_{int}^{sat} = \pm P M_s$, that leads, for a constant M_s, to a temperature-independent $\left|H_{int,FORC}^{sat}\right|$ amplitude, as observed experimentally for both samples (Fig. 1(f), 2(f)). Moreover, the measured interaction field at saturation scales with P with larger values for sample *A*. These points indicate a dominant mean field interaction regime, also evidenced by the presence of the wishbone shape in the diagrams and by the constant ρ_{FORC} profiles along the IFD [18,19,20,21,22], both being signatures of this regime. Interestingly, some deviations from a pure mean field description of interactions can be then identified. First, the moving Preisach model predicts $H_{int}^{zz} = 0$ at $M = 0$, while the measurements indicate $H_c^{mean} \geq H_c^{MHL}$ due to persistent interactions near the demagnetized state. Then, IFD of sample *T* at 300K and 200K presents peaked IFD profiles, a signature of an inhomogeneous interaction field [22,34]. This means that sample *T* presents a significantly larger deviation of the interaction field $\sigma_{H_{int}}$ in comparison to sample A, which could be related to the bending and bundling of these small diameter nanowires (Fig. 2(a)).

Quantitative analysis of FORC diagrams beyond the classical Preisach model showed that the standard deviation of a gaussian SFD in a dipolar coupled assembly of nanomagnets can be accurately approached from the coordinates of A and B points of the diagram as $\sigma_{H_{sw}} = \frac{H_c^{mean} - H_c^{min}}{3}$ [18,22]. The corresponding $\sigma_{H_{sw}}$ values obtained from the FORC analysis are plotted as a function of temperature on Fig. 5(a). As expected qualitatively from the transition between linear and wishbone diagrams, the intrinsic SFD deviation increases at low temperatures. Analysis of the coercive field as a function of temperature has showed that the energy barrier involved in the magnetization reversal is composed of shape anisotropy and temperature-dependent magnetocrystalline anisotropy of *hcp* Co, despite being of lower amplitudes than predicted from the bulk values. In such a real system, local structural defects in the *hcp* structure of Co, such as stacking faults, would intrinsically reduce the anisotropy; for instance, this would result in local *fcc* stackings, whose magnetocrystalline anisotropy is one order of magnitude smaller than for *hcp* with very little temperature dependence [50]. Hence, the contrast in the anisotropy amplitudes between pure *hcp* crystallites and crystallites with defects would increase at low temperatures, broadening the switching field distribution. As the temperature-dependence of the *hcp* magnetocrystalline anisotropy is responsible for the increase at low temperatures of both the coercive field and SFD deviation, the measured relative dispersion σ_{Hsw}/H_C^{MHL} is therefore found almost constant at 20% on the studied temperature range (Fig. 5(b)).

Generally, the SFD deviation increases when decreasing the nanomagnet size because the properties are averaged over less magnetic volume in small elements. With nanowire diameters of 6.3 nm (sample *T*) and 12.5 nm (sample *A*), the pitch of these arrays reaches 8 nm and 15 nm, respectively. Focusing on future generation of magnetic media, namely bit patterned media, the present system synthesized by a pure bottom-up process reaches pitch values yet unachievable by top-down approaches. It is particularly interesting to note that the reported value follows the general trend observed of SFDs in state-of-the-art BPM, when extrapolated to the present pitch [2].

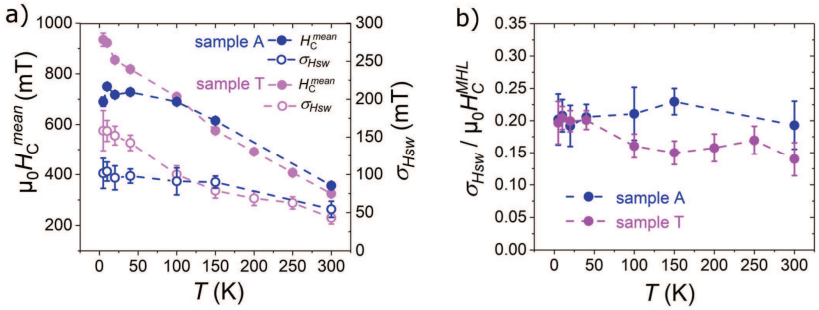

Figure 5: FORC analysis - a) H_c^{mean} (left) and σ_{Hsw} (right) extracted from FORC diagrams of samples *A* and *T*. b) Relative switching field distributions σ_{Hsw}/H_c^{MHL} for both samples.

In conclusion, we have conducted the analysis of the switching field distribution of ultra-dense arrays of magnetic nanowires that fulfill strategical prerequisites of bit patterned media such as bottom-up synthesis of single-crystalline nano-elements self-organized in 2D dense superlattices. Particularly, the hard-magnetic behaviour provided by combined uniaxial shape and magnetocrystalline anisotropies allow to maintain perpendicular magnetic anisotropy despite important dipolar interactions with densities of 10×10^{12} NWs/in². Qualitative and quantitative analysis of temperature-dependent FORC allows concluding that the self-organized nanowire arrays exhibit dipolar interaction of a dominant mean field character accompanied with some noticeable deviations. We have shown that both the coercive and mean switching fields originates from thermal relaxation with an energy barrier composed of shape and temperature-dependent Co *hcp* magnetocrystalline anisotropies smaller than expected from bulk arguments. As a consequence, the deviation of the intrinsic switching field distribution increases at low temperatures, while its normalized value to coercive field keeps constant. These results suggest the possibility of improving the synthesis procedure to bring this promising technology to the level of technical maturity needed for magnetic recording applications.

Acknowledgements

This work was supported by the Agence Nationale de la Recherche (France) under contract No. ANR-14-CE07-0025-01 (DENSAR) and by the Programme Investissements d'Avenir under the programme ANR-11-IDEX-002-02, ref. ANR-10-LABX-0037-NEXT. This study has been partially supported through the EUR grant NanoX n° ANR-17-EURE-0009 in the framework of the « Programme des Investissements d'Avenir".

AUTHOR DECLARATIONS

Conflict of Interest

The authors have no conflicts to disclose.

Author Contributions

Alexandre Pierrot: Investigation (equal); Data curation; Software; Formal Analysis; Writing – review and editing (equal). Deliang Yi: Investigation (equal). Laurent Peres: Investigation (supporting). Katerina Soulantica: Conceptualization; Supervision; Writing – review and editing (equal). Robin Cours:

Investigation. Bénédicte Warot-Fonrose: Investigation; Writing – review and editing (equal). Cécile Marcelot: Investigation. Marc Respaud: Conceptualization. Fanny Béron: Validation; Methodology; Software. Thomas Blon: Conceptualization; Funding acquisition; Investigation (equal); Supervision; Writing – original draft; Writing – review and editing (equal).

DATA AVAILABILITY

The data that support the findings of this study are available from the corresponding author upon reasonable request.

References

[1] T. Thurn-Albrecht, J. Schotter, G.A. Kästle, N. Emley, T. Shibauchi, L. Krusin-Elbaum, K. Guarini, C.T. Black, M.T. Tuominen, T.P. Russell, *Science* **290**, 2126 (2000)

[2] T.R. Albrecht, H. Arora, V. Ayanoor-Vitikkate, J-M. Beaujour, D. Bedau, D. Berman, A.L. Bogdanov, Y-A. Chapuis, J. Cushen, E.E. Dobisz., *IEEE Trans. Magn.* **51**, 1 (2015)

[3] S.H. Sun, C.B. Murray, D. Weller, L. Folks, A. Moser, *Science* **287**, 1989 (2000)

[4] L. Piraux, *Appl. Sci.* **10**(5), 1832 (2020)

[5] A. Encinas, L. Vila, M. Darques, J-M. George, L. Piraux *Nanotechnology* **18** 065705 (2007)

[6] T. Blon, M. Mátéfi-Tempfli, S. Mátéfi-Tempfli, L. Piraux, S. Fusil, R. Guillemet, K. Bouzehouane, C. Deranlot, V. Cros, *J. Appl. Phys.* **102**, 103906 (2007)

[7] J.M. Martínez-Huerta, J De La Torre Medina, L Piraux, A Encinas, *J. Phys.: Condens. Matter.* **25**, 226003 (2013)

[8] M.R.Z. Kouhpanji, B.J.H. Stadler, *Nano Express* **1**, 010017 (2020)

[9] O. Dmytriiev, U. A. S. Al-Jarah, P. Gangmei, V. V. Kruglyak, R. J. Hicken, B. K. Mahato, B. Rana, M. Agrawal, A. Barman, M. Mátéfi-Tempfli L. Piraux, S. Mátéfi -Tempfli, *Phys. Rev. B* **87**, 174429 (2013)

[10] N. Liakakos, C. Achkar, B. Cormary, J. Harmel, B. Warot-Fonrose, E. Snoeck, B. Chaudret, M. Respaud, K. Soulantica, T. Blon, *ACS Nano* **9**, 9665 (2015)

[11] D. Yi, L. Peres, A. Pierrot, S. Cayez, R. Cours, B. Warot-Fonrose, C. Marcelot, P. Roblin, K. Soulantica, T. Blon, *Nano Res. 10.1007/s12274-022-4804-6* (2022)

[12] N. Liakakos, T. Blon, C. Achkar, V. Vilar, B. Cormary, R.P. Tan, O. Benamara, G. Chaboussant, F. Ott, B. Warot-Fonrose, E. Snoeck, B. Chaudret, K. Soulantica, M. Respaud, *Nano Lett.* **14** 3481 (2014)

[13] I.S. Camara, C. Achkar, N. Liakakos, A. Pierrot, V. Pierron-Bohnes, Y. Henry, K. Soulantica, M. Respaud, T. Blon, M. Bailleul, *Appl. Phys. Lett.* **109** 202406 (2016)

[14] I. Tagawa, Y. Nakamura, *IEEE Trans. Mag*. **27** 4975 (1991)

[15] A. Berger, B. Lengsfield, Y. Ikeda, *J. Appl. Phys.* **99**, 08E705 (2006)

[16] T. Hauet, L. Piraux, S.K. Srivastava, V.A. Antohe, D. Lacour, M. Hehn, F. Montaigne, J. Schwenk, M.A. Marioni, H.J. Hug, O. Hovorka, A. Berger, S. Mangin, F. Abreu Araujo, *Phys. Rev. B* **89**, 174421 (2014)

[17] J. M. Martínez Huerta, J. De La Torre Medina, L. Piraux, A. Encinas, *J. Appl. Phys.* **111**, 083914 (2012)

[18] C.-I. Dobrotă, A. Stancu, *J. Appl. Phys.* **113**, 043928 (2013)

[19] A.P. Roberts, D. Heslop, X. Zhao, C.R. Pike, *Rev. Geophys.* **52**, 557 (2014)

[20] D.A. Gilbert, G.T. Zimanyi, R.K Dumas, M. Winklhofer, A. Gomez, N. Eibagi, J.L. Vicent, K. Liu, *Sci. Rep.* **4**, 4204 (2014)

[21] S. Ruta, O. Hovorka, P.-W. Huang, K. Wang, G. Ju, R. Chantrell, *Sci. Rep.* **7**, 45218 (2017)

[22] A. Pierrot, F. Béron, T. Blon, *J. Appl. Phys.* **128**, 093903 (2020)

[23] K. Soulantica, F. Wetz, J. Maynadié, A. Falqui, R. P. Tan, T. Blon, B. Chaudret, M. Respaud, *Appl. Phys. Lett.* **95**, 152504 (2009)

[24] O. Benamara, E. Snoeck, M. Respaud, T. Blon, *Surf. Sci.* **605** 1906–1912 (2011)

[25] M.P. Sharrock, *J. Appl. Phys.* **76**, 6413 (1994)

[26] F. Ono, H. Maeta, *Physica B* **161**, 134 (1989)

[27] H. Zeng, R. Skomski, L. Menon, Y. Liu, S. Bandyopadhyay, D.J. Sellmyer, *Phys. Rev. B* **65**, 134426 (2002)

[28] W. Wernsdorfer, E. Bonet Orozco, K. Hasselbach, A. Benoit, B. Barbara, N. Demoncy, A. Loiseau, H. Pascard, D. Mailly, *Phys. Rev. Lett.* **78**, 1791 (1997)

[29] S. Wirth, M. Field, D. D. Awschalom, S. Von Molnár, *Phys. Rev. B* **57**, R14028 (1998)

[30] P.M. Paulus, F. Luis, M. Kröll, G. Schmid, L.J. de Jongh, *J. Mag. Mag. Mat.* **224**, 180 (2001)

[31] F. Vidal, Y. Zheng, P. Schio, F.J. Bonilla, M. Barturen, J. Milano, D. Demaille, E. Fonda, A.J.A. de Oliveira, V.H. Etgens, *Phys. Rev. Lett.* **109**, 117205 (2012)

[32] P. Sergelius, J. G. Fernandez, S. Martens, M. Zocher, T. Böhnert, V. V. Martinez, V. Manuel de la Prida, D. Görlitz, K. Nielsch, *J. Phys. D: Appl. Phys.* **49**(14), 145005 (2016)

[33] L. Spinu, A. Stancu, C. Radu, F. Li, J.B. Wiley, *IEEE Trans. Magn.* **40**, 2116 (2004)

[34] F. Béron, L. Clime, M. Ciureanu, D. Ménard, R.W. Cochrane, A. Yelon, J. *Nanosci. Nanotechnol.* **8**(6), 2944 (2008)

[35] F. Béron, D. Ménard, A. Yelon, *J. Appl. Phys.* **103**(7), 07D908 (2008)

[36] R. Lavin, J.C. Denardin, J. Escrig, D. Altbir, A. Cortes, H. Gomez, *IEEE Trans. Magn.* **44**(11), 2808 (2008)

[37] S. Samanifar, M. A. Kashi, A. Ramazani, *Phys. C Supercond. Its Appl.* **548**, 72 (2018)

[38] X. Kou, X. Fan, R.K. Dumas, Q. Lu , Y. Zhang, H. Zhu, X. Zhang, K. Liu, J.Q. Xiao, *Adv. Mater.* **23**(11), 1393 (2011).

[39] M.P. Proenca , C. T. Sousa, J. Ventura, J. Garcia, M. Vazquez, J.P. Araujo, *J. Alloys Compd.* **699**, 421 (2017)

[40] L.C.C. Arzuza, R. López-Ruiz, D. Salazar-Aravena, M. Knobel, F. Béron, K.R. Pirota, *J. Magn. Magn. Mater.* **432**, 309 (2017)

[41] A. Ramazani, V. Asgari, A. H. Montazer, M. Almasi Kashi, *Curr. Appl. Phys.* **15**(7), 819 (2015)

[42] V. Vega, J. García, W.O. Rosa, L.G. Vivas, V.M. Prida, B. Hernando, M. Vázquez, *J. Nanosci. Nanotechnol.* **12**(6), 4736 (2012)

[43] T.R.F. Peixoto, D.R. Cornejo, *J. Magn. Magn. Mater.* **320**(14), e279 (2008)

[44] C. R. Pike, C. A. Ross, R. T. Scalettar, G. Zimanyi, *Phys. Rev. B* **71**, 134407 (2005)

[45] R. Hertel, *J. Appl. Phys.* 90, 5752 (2001)

[46] F. Zighem, T. Maurer, F. Ott, G. Chaboussant, *J. Appl. Phys.* 109, 013910 (2011)

[47] E. Della Torre, *IEEE Trans. Audio* **AU-14**, 86 (1966)

[48] L.-P. Carignan, C. Lacroix, A. Ouimet, M. Ciureanu, A. Yelon, D. Ménard*, J. Appl. Phys.* **102**, 023905 (2007)

[49] S. Vock, C. Hengst, Z. Sasvári, R. Schäfer, L. Schultz, V. Neu, *J. Phys. D: Appl. Phys.* **50**, 475002 (2017)

[50] T. Suzuki, D. Weller, C.-A. Chang, R. Savoy, T. Huang, B.A. Gurney, V. Speriosu, *Appl. Phys. Lett.* **64**, 2736 (1994)